Superconductor Science and Technology

PAPER

Influence of strain-driven segregation in low-angle grain boundaries on critical current density of $Y_{0.9}Nd_{0.1}Ba_2Cu_3O_{7-d}$

To cite this article: Sang-il Kim and David C Larbalestier 2021 *Supercond. Sci. Technol.* **34** 025008

IOP Publishing Superconductor Science and Technology
Supercond. Sci. Technol. 34 (2021) 025008 (8pp) https://doi.org/10.1088/1361-6668/abc8d1

Influence of strain-driven segregation in low-angle grain boundaries on critical current density of $Y_{0.9}Nd_{0.1}Ba_2Cu_3O_{7-d}$

Sang-il Kim[1] **and David C Larbalestier**[2]

[1] Department of Materials Science and Engineering, University of Seoul, Seoul 02504, Republic of Korea
[2] National High Magnetic Field Laboratory, Florida State University, Tallahassee, FL 32310, United States of America

E-mail: larbalestier@asc.magnet.fsu.edu

Received 21 September 2020, revised 27 October 2020
Accepted for publication 9 November 2020
Published 11 January 2021

Abstract

Low-angle grain boundaries (GBs) constitute the most important current-limiting mechanism in the operation of biaxially textured $YBa_2Cu_3O_{7-d}$ (YBCO)-coated conductors. Ca doping of YBCO is known to improve the critical current density J_c across the GB because of carrier doping by anisovalent Ca^{2+} substitution for Y^{3+} and the strain relief induced by Ca segregation at the GB cores; however, the reduction of the superconducting critical temperature T_c accompanying such doping is a marked drawback. Here we study the substitution of isovalent Nd^{3+} for Y^{3+} again using strain-driven segregation, in this case Nd^{3+}, to improve J_c without incurring significant T_c reduction. Transport characteristics of low-angle GBs of 10% Nd-doped YBCO, $Y_{0.9}Nd_{0.1}Ba_2Cu_3O_{7-d}$, grown on single crystal and 6° and 9° [001] tilt symmetric bicrystal $SrTiO_3$ substrates are reported. It was found that J_c across the 6° GB recovers to the intra-grain J_c value in the 10% Nd-doped YBCO, while the 9° GB shows a modest J_c enhancement compared to the pure YBCO 9° GB without a significant T_c reduction. It is shown that the transparency of the GB could be enhanced without a large T_c reduction by the isovalent substitution of rare-earth ions, suggesting new opportunities for cation segregation engineering in YBCO by isovalent rare-earth substitution.

Supplementary material for this article is available online

Keywords: critical current density, grain boundary, segregation, superconductivity, coated conductors

(Some figures may appear in colour only in the online journal)

1. Introduction

Low-angle grain boundaries (GBs) are the most important current-limiting mechanism in the operation of biaxially textured $YBa_2Cu_3O_{7-d}$ (YBCO)-coated conductors (CCs) because the critical current density J_c decreases with increasing GB misorientation angle θ [1–5]. Despite improvements in the texture of YBCO-coated conductors prepared by the rolling assisted bi-axially textured substrate (RABiTS) route to the full-width half-maximum (FWHM) of approximately 4–6°, a previous study on the current-limiting mechanisms of the GB network in real metal organic deposition CCs showed that even the best CC prepared to date on RABiTS have their low-field J_c limited by the GB network [6, 7]. Although IBAD (ion beam assisted deposition)-MgO template CC has a smaller FWHM misorientation of 3–5°, there is always an advantage to enhance the J_c properties of low-angle GBs.

Low-angle GBs are composed of an array of alternating superconducting channels and weakly superconducting, under-doped, or even insulating GB dislocation cores [8–10]. GB transparency is known to be enhanced by Ca substitution due to the carrier doping by the anisovalent

substitution of Ca^{2+} for Y^{3+} and the strain relief induced by the Ca segregation at the GB cores [11–15]. However, Ca doping is also accompanied by a substantial decrease in superconducting critical temperature T_c due to the over-doping of the YBCO grains. Consequently, J_c improvement at the higher temperatures, where applications are most desirable, is less than initially expected. In an earlier paper we explored GB engineering with one of the smallest rare earth ions, Yb [16]. For Ca-doped YBCO, it was shown that $J_{c,gb}$ can even exceed the intra-grain J_c at high field and low temperature where the pinning by GB dislocations can be optimized [16]. However, the T_c reduction imposed by Ca doping is still a major drawback to its use in real applications.

To prevent large T_c reduction, we here investigate strain-driven segregation of the isovalent Nd^{3+} RE ion at the GB cores. Nd-doped YBCO has been investigated to modify the intra-grain J_c [17, 18], however, J_c across low-angle GBs has not been studied. The pressure fields around the GB dislocation cores is expected to drive the larger Nd^{3+} ions to segregate to the lower density regions of the GB cores to minimize the GB strain field. Therefore, we speculated that J_c across low-angle GBs could be enhanced without incurring a significant T_c reduction in the Nd-doped YBCO. In this paper, a thorough analysis of the GBs of 10% Nd-doped YBCO ($Y_{0.9}Nd_{0.1}Ba_2Cu_3O_{7-d}$) is reported.

We used the cation segregation model proposed by Gurevich [19] in which Cottrell atmospheres of the substituted ions form under the combined effects of the strain [19, 20] and electric fields of the dislocations [21, 22]. This model allowed us to predict a means by which J_c could be enhanced by 10% Nd doping. The driving force for the segregation, in this case, is the size difference between Y^{3+} and Nd^{3+} without the valence difference. The segregation at the GB dislocation core with depleted charge carriers due to strains would relive strains by the expansion of the core, enhancing charge carrier density, thereby causing the transport properties to change according to the doping level. Thus, the larger Nd^{3+} ions segregate to the tensile regions of the GB dislocations, and are depleted in the compressed regions

2. Experimental details

Films were grown by pulsed laser deposition from a target of the nominal composition of $Y_{0.9}Nd_{0.1}Ba_2Cu_3O_{7-d}$ on single crystal $SrTiO_3$ (STO) and on symmetric 6° and 9° [001] tilt bicrystal STO substrates. The substrate temperature was set to 800 °C–810 °C during the growth. The changes of the oxygen pressure (P_{O2}) to 300, 250, and 200 mTorr during growth gave rise to different values of T_c (table 1) due to different oxygen deficiency d and possible antisite defects induced by the substitution of Ba^{2+} by Nd^{3+} [23]. T_c is generally decreased with decreasing P_{O2} for all films. The films grown at P_{O2} of 300 mTorr showed T_c of 87 K–88 K, which was the highest T_c among the films investigated in this study. The films grown with P_{O2} of either 250 mTorr or 200 mTorr exhibited lower T_c values of approximately 86 K and ~85 K, respectively. A total of 5000 pulses at 5 Hz were used to deposit approximately 300 nm thick films.

Table 1. T_c values of the Nd-doped samples for different oxygen partial pressures.

Misorientation angle	300 mTorr	250 mTorr	200 mTorr
0°	88.0 K	85.8 K	85.5 K
6°	87.2 K	86.5 K	84.2 K
9°	—	84.5 K	83.5 K

Bridges of 40 μm (width) × 1000 μm (length) were cut by Nd-YAG (yttrium aluminum garnet) laser ablation for all samples in order to perform detailed transport measurements. The *V–I* characteristics were obtained with standard four-point measurements, while a current reversal algorithm was employed to remove thermal voltages. The measurements were performed at 77 K and at the same reduced temperature $t \sim T_m/T_c$ (T_m is the measurement temperature) of 0.85 for comparison, because T_c varies according to the Nd content and oxygen annealing condition. For the samples grown at 250 mTorr, the *V–I* measurements were also performed at 65 K.

A current pulse of 50 ms duration and voltage read time of 30 ms was used for currents higher than 100 mA to prevent possible sample heating. The measurements were performed over a wide range of magnetic fields up to 12 T applied perpendicularly to the film surface in an OXFORD magnet system. The values of J_c were determined using an electric field criterion of 1 μV cm^{-1}.

3. Experimental results

3.1. Growth of $Y_{0.9}Nd_{0.1}Ba_2Cu_3O_{7-d}$ at P_{O2} = 300 mTorr

The T_c values were 88.0 K and 87.2 K for the 0° and 6° $Y_{0.9}Nd_{0.1}Ba_2Cu_3O_{7-d}$ films grown with a P_{O2} of 300 mTorr, respectively, the highest among all samples grown under a variety of P_{O2} conditions. Figure 1 shows the $J_c(H)$ results for the samples at a reduced temperature $t = T_m/T_c \sim 0.85$ and at 77 K. Given that the Nd doping is accompanied by a modest T_c reduction of a few degrees Kelvin (possibly due to partial Nd/Ba site exchange [21]), the relative J_c(H) improvement was evaluated at constant reduced temperature. The value of J_c across the 6° GB is reduced at magnetic fields less than 3–4 T compared to its intra-grain J_c but the reduction is smaller than in similarly grown pure YBCO bicrystal films, as shown for the $J_c(H)$ characteristics of the 6° YBCO GB (figures 1(a) and (b)). Figures 1(c) and (d) present the *V–I* characteristics of the 6° GB at $t \sim 0.85$ and at 77 K, respectively. Both show the knee that is characteristic of the transition from GB-limited transport at lower fields to removal of the GB limit at higher fields.

3.2. Growth of $Y_{0.9}Nd_{0.1}Ba_2Cu_3O_{7-d}$ at 250 mTorr

The T_c values for films grown with 250 mTorr were slightly lower than those grown with P_{O2} = 300 mTorr, 85.8 K,

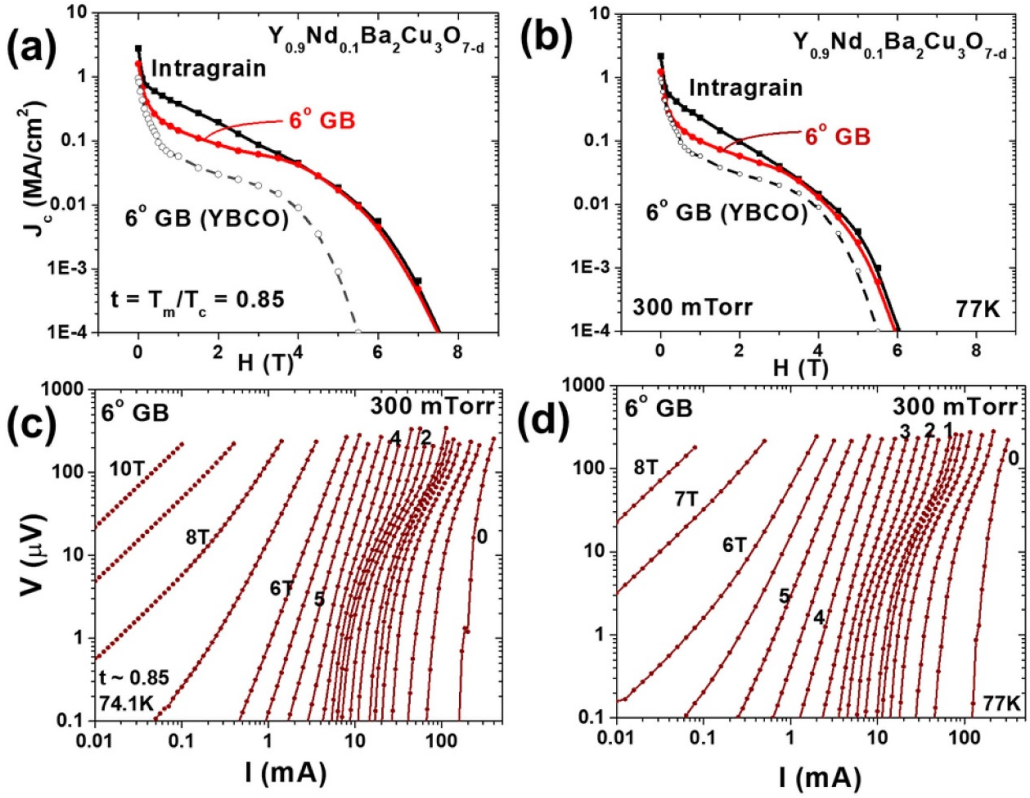

Figure 1. (a) and (b) $J_c(H)$ of the intra-grain and the 6° GB of $Y_{0.9}Nd_{0.1}Ba_2Cu_3O_{7-d}$ grown in P_{O2} of 300 mTorr, ($J_c(H)$ of the 6° GB of YBCO is also shown for comparison) (a) at reduced temperature $t \sim 0.85$ and (b) at 77 K. The 6° GB shows reduced $J_{c,gb}$ in fields of less than 3.5–4.0 T. The behavior is not significantly different from that of pure YBCO. No distinctive improvement in the GB properties is observed and the T_c values were 88.0 K and 87.2 K for the 0° and 6° $Y_{0.9}Nd_{0.1}Ba_2Cu_3O_{7-d}$ films; (c) and (d) V–I characteristics of the 6° $Y_{0.9}Nd_{0.1}Ba_2Cu_3O_{7-d}$ film grown in 300 mTorr for GB (c) at $t \sim 0.85$ and (d) at 77 K. GB dissipation signature is highlighted with yellowish regions.

86.5 K, and 84.5 K for the 0°, 6°, and 9° films, respectively, making the 77 K J_c values and irreversibility fields H_{irr} lower too. Figures 2(a) and (b) show the $J_c(H)$ results at $t \sim 0.85$ and at 77 K, respectively. In figure 2(a), the 6° $Y_{0.9}Nd_{0.1}Ba_2Cu_3O_{7-d}$ GB shows a large J_c improvement over the entire field range compared to the 6° pure YBCO GB. Indeed, J_c across the GB recovered the intra-grain J_c values. Furthermore, the 9° $Y_{0.9}Nd_{0.1}Ba_2Cu_3O_{7-d}$ GB also exhibits a significantly improved J_c, compared to the 9° pure YBCO GB. In figure 2(b), the intra-grain and the 6° GB $J_c(H)$ are almost identical at 77 K, while the 9° GB shows a reduction of J_c across the GB. It is even more promising that Nd doping has a remarkable positive effect both on the 6° and 9° GBs with only a slight T_c reduction. (T_c is ~85 K–86 K) figures 2(c)–(h) depicts the V–I characteristics of the $Y_{0.9}Nd_{0.1}Ba_2Cu_3O_{7-d}$ samples grown at 250 mTorr. Consistent with the agreement of inter-grain and grain J_c values, there was a complete absence of GB signature for the 10% Nd-doped YBCO for the 6° GB at 77 K. However, a small GB dissipation signature is found for the 6° $Y_{0.9}Nd_{0.1}Ba_2Cu_3O_{7-d}$ GB at a lower temperature of 73.5 K corresponding to $t \sim 0.85$ (figure 2(g)).

Figure 3 shows the $J_c(H)$ values of the $Y_{0.9}Nd_{0.1}Ba_2Cu_3O_{7-d}$ films containing 0°, 6°, and 9° GBs at 65 K. For the 6° GB, compared to the intra-grain J_c, $J_c(H)$ has slightly lower values at fields lower than 6 T. Even though a complete loss of the GB signature was observed at 77 K (figure 2(d)), a slight GB dissipation signature recurs at temperatures lower than 65 K, as shown in figure 3(b). Typically, the GB blocking effect increases with decreasing temperature [24]. The 9° GB shows a large reduction in J_c at all fields.

3.3. Growth of $Y_{0.9}Nd_{0.1}Ba_2Cu_3O_{7-d\delta}$ at 200 mTorr

Lastly, we grew a set of $Y_{0.9}Nd_{0.1}Ba_2Cu_3O_{7-d}$ films at P_{O2} of 200 mTorr, finding that T_c values for the 0°, 6°, and 9° samples were 85.5 K, 84.2 K, and 83.5 K, again slightly reduced by the lower P_{O2}. Figure 4(a) depicts the intra-grain and the inter-grain 6° GB $J_c(H)$ characteristics at $t \sim 0.85$ are identical, indicating no suppression of inter-grain J_c(H), in marked contrast to the suppression of inter-grain J_c(H) seen for the pure 6° YBCO GB. The enhancement of GB transport ($J_{c,gb}$) is observed explicitly for this 10% Nd-doped YBCO. Figure 4(b) presents $J_c(H)$ of the $Y_{0.9}Nd_{0.1}Ba_2Cu_3O_{7-d}$ film for the 9° GB at $t \sim 0.85$, comparing it to the pure 9° YBCO GB and 9° GB made with 10% Ca-doped YBCO, which is grown at the same P_{O2} of 200 mTorr [24]. The $J_{c,gb}$ across the 9° GB in the Nd doped film is greatly improved by a factor of ~5 in this case. (We note that 9° GB of 10% Ca-doped YBCO exhibited minimal J_c enhancement at low

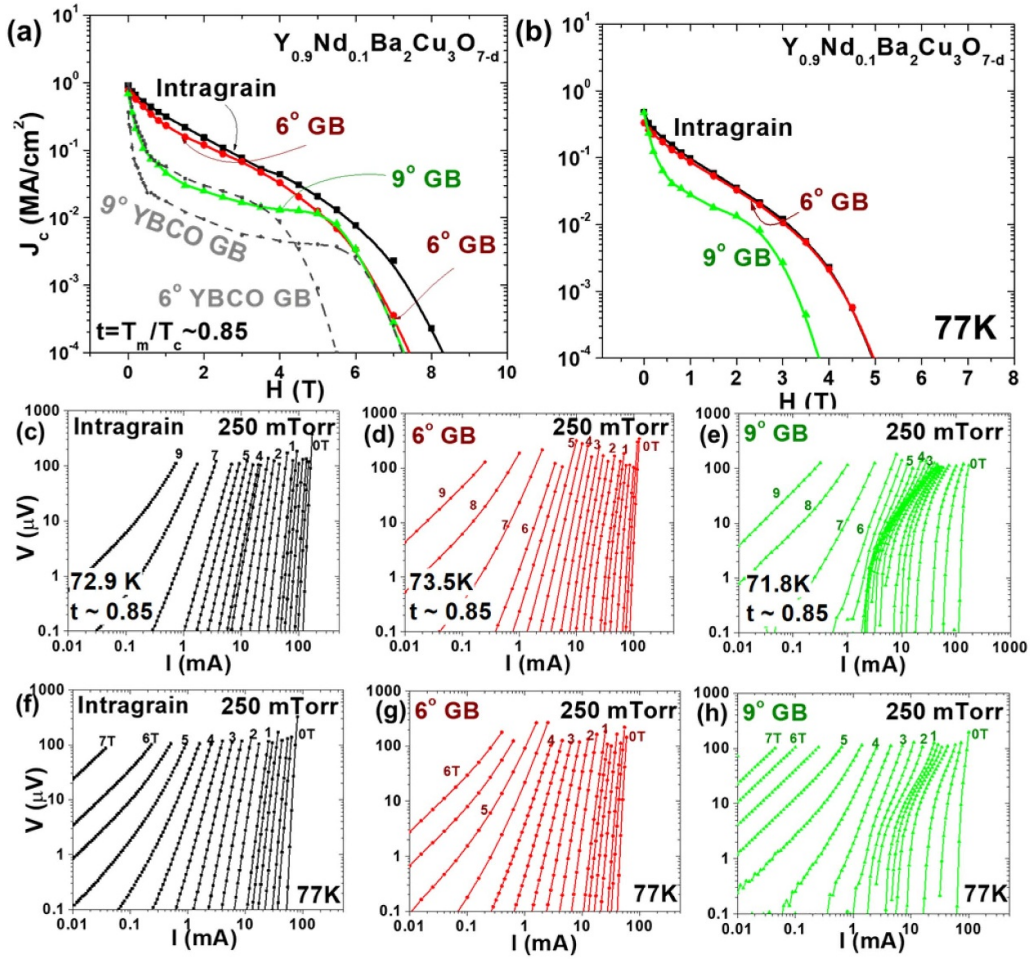

Figure 2. (a) and (b) $J_c(H)$ of the intra-grain, 6°, and 9° GB of the $Y_{0.9}Nd_{0.1}Ba_2Cu_3O_{7-d}$ films grown in P_{O2} of 250 mTorr (a) at $t \sim 0.85$ and (b) at 77 K. The intra-grain and 6° GB $J_c(H)$ results are almost identical. The $J_c(H)$ data for the 6° and 9° YBCO GB at $t \sim 0.85$ are also plotted for comparison. The T_c values of the samples grown in P_{O2} of 250 mTorr are 85.8 K, 86.5 K and 84.5 K for the 0°, 6° and 9° samples, respectively. (c)–(h) *V–I* characteristics of $Y_{0.9}Nd_{0.1}Ba_2Cu_3O_{7-d}$ grown at P_{O2} of 250 mTorr for (c) 0°, (d) 6° and (e) 9° GB at $t \sim 0.85$, and for (f) 0°, (g) 6° and (h) 9° GB at 77 K. No strong GB dissipation signature is observed for the 6° GBs. There is indeed no significant difference between the intra-grain and 6° GB *V–I* curves. GB dissipation signature is highlighted with yellowish regions.

fields.) figures 4(c)–(e) show the intra-grain, 6° GB, and 9° GB *V–I* characteristics for the 10% Nd-doped YBCO grown at 200 mTorr. A complete loss of the GB signature is observed in figure 4(d) for the 6° $Y_{0.9}Nd_{0.1}Ba_2Cu_3O_{7-d}$ GB. Even though a strong GB signature is present in the *V–I* characteristics of the 9° $Y_{0.9}Nd_{0.1}Ba_2Cu_3O_{7-d}$ GB, based on to the improvement in J_c shown in figure 4(b), the GB dissipation is notably reduced compared to that observed in pure YBCO and 9° YBCO GB.

4. Discussion

The basis for this study was that the size difference between the Y^{3+} and Nd^{3+} ions would allow Nd^{3+} segregation at the GB dislocation cores, thus enabling a reduction of the lattice distortion in the Nd-doped YBCO GB that would reduce the strain at the GB cores, leading to enhanced GB transparency. Moreover, compared to Ca doping, we hypothesized that Nd^{3+} doping would decrease T_c much less significantly when Nd^{3+} substituted for Y^{3+}. Thus, Nd^{3+} doping in YBCO was proposed to improve the $J_{c,gb}$ properties without incurring significant T_c reduction. Indeed we observed an improved inter-grain J_c, and a weaker or removed GB dissipation signature. As we now discuss, we find that the experimental data on the Nd-doped bicrystal YBCO films can be illuminated by the segregation modeling [19]. These results are reasonably explained by the expected enhanced carrier density at the GB dislocation cores induced by the strong Nd segregation to the GB.

The cation segregation model of Gurevich [19] predicts that Cottrell atmospheres of the dopant ions form under the combined effects of the strain and electric fields of the dislocations generated in a low-angle GB. In our earlier studies, we found that this model successfully described the observed non-uniform Ca distribution along and across the GBs in Ca-doped YBCO. In the present work, we used the model to predict the Nd concentration $c(x,y)$ at the GB. In the model, the equilibrium concentration $c(x,y)$ of the dopant in *the* pressure field $p(x,y)$ and the screened electric potential $\varphi(r)$ produced by the GB dislocation is given by:

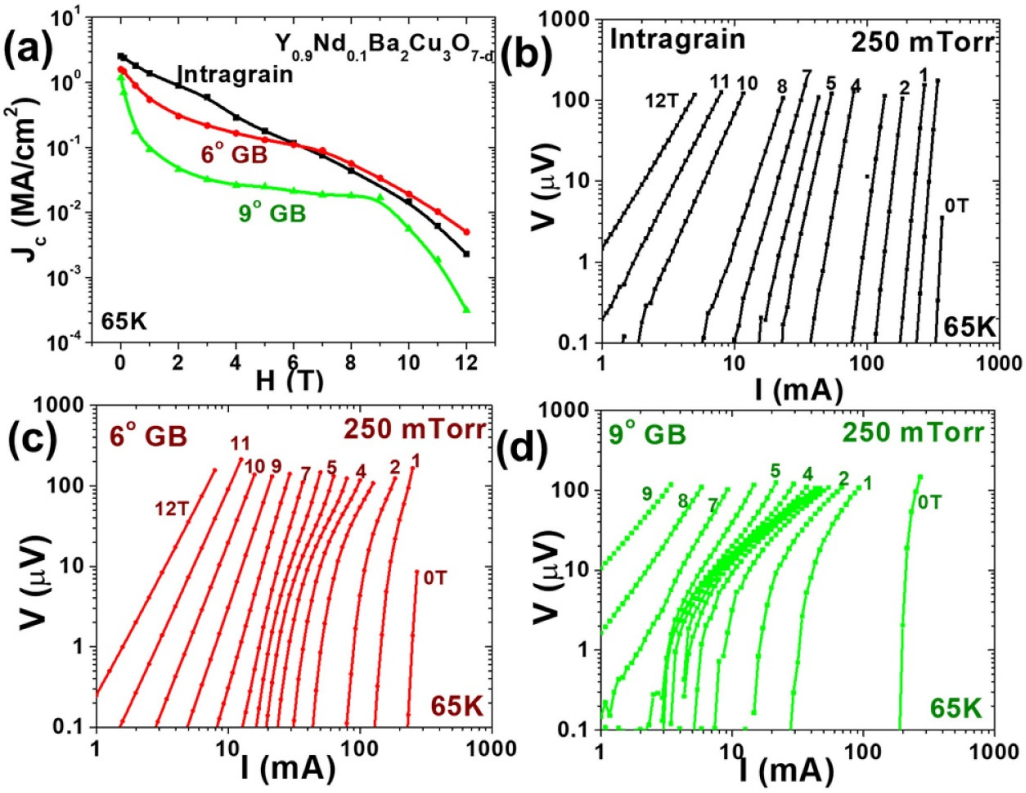

Figure 3. (a) $J_c(H)$ results for the intra-grain, 6°, and 9° GB of the $Y_{0.9}Nd_{0.1}Ba_2Cu_3O_{7-d}$ samples grown at P_{O2} of 250 mTorr at 65 K; $J_c(H)$ of the 6° GB shows a reduction at a lower field. This is reasonable because the GB effect becomes stronger with decreasing temperature. (b)–(d) *V–I* characteristics of $Y_{0.9}Nd_{0.1}Ba_2Cu_3O_{7-d}$ grown in P_{O2} of 250 mTorr for (b) 0°, (c) 6° and (d)9° GB at 65 K. The *V–I* curves of the 6° GB exhibit a GB signature at 65 K.

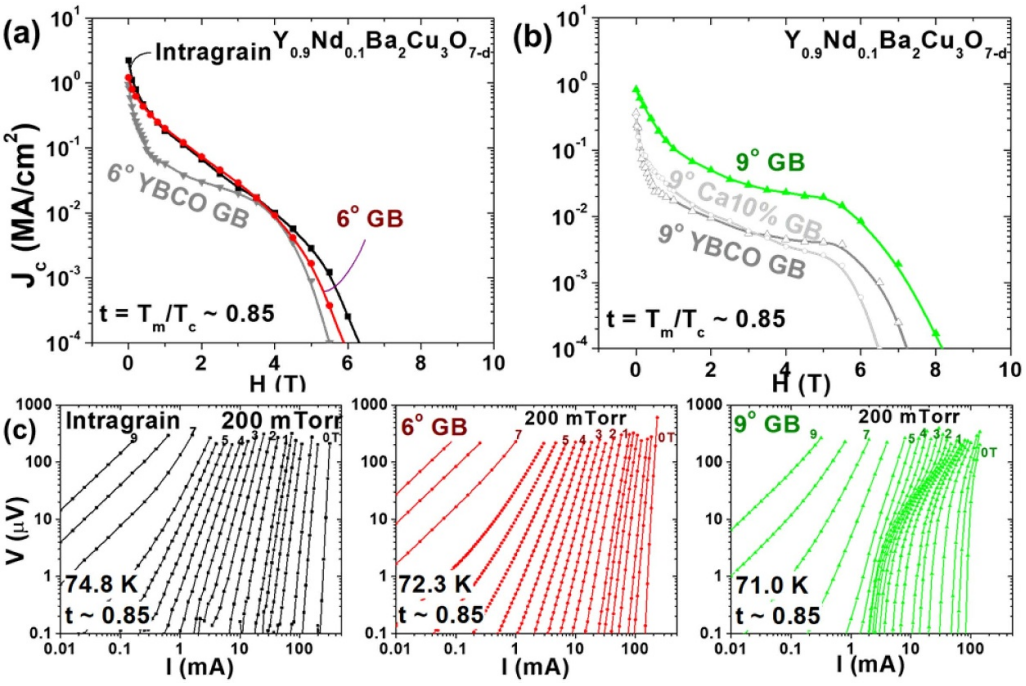

Figure 4. (a) $J_c(H)$ of the intra-grain and 6° GB of the $Y_{0.9}Nd_{0.1}Ba_2Cu_3O_{7-d}$ films grown at P_{O2} of 200 mTorr at $t \sim 0.85$; $J_c(H)$ of 6° YBCO GB was shown for comparison. Clear enhancement of J_c occurs at low field; (b) $J_c(H)$ of the 9° GB of $Y_{0.9}Nd_{0.1}Ba_2Cu_3O_{7-d}$ films grown at 200 mTorr at $t \sim 0.85$; $J_c(H)$ data of the 9° YBCO GB and 9° GB of 10% Ca-doped YBCO [22] are shown for comparison; (c)–(e) V–I characteristics of the $Y_{0.9}Nd_{0.1}Ba_2Cu_3O_{7-d}$ films grown at 200 mTorr for (c) 0°, (d) 6° and (e) 9° GB at $t \sim 0.85$. The *V–I* curves of the 6° GB show no GB signature.

$$c = \frac{c_0}{c_0 + (1 - c_0)\exp[(p\Delta V + \phi\Delta Z)/k_B T]} \quad (1)$$

where $\Delta V = V_{Dopant} - V_Y$ and $\Delta Z = Z_{Dopant} - Z_Y$ are the differences in the ionic volume and charge of the dopant and substituted Y, c_0 is the bulk concentration, $p(x,y) = p_0 \sin(2\pi y/d)/[\cosh(2\pi\rho/d) - \cos(2\pi y/d)]$, $d = b/2\sin(\theta/2)$, $p_0 = \mu\sin(\theta/2)/(1-\nu)$, $\rho = (r_0^2 + x^2)^{1/2}$, the cut-off radius $r_0 \sim b$ accounts for the plastically deformed dislocation core, μ is the shear modulus, ν is the Poisson ratio, k_B is the Boltzmann constant, and x and y are the coordinates across and along the GB, respectively. In the case of Nd doping with $\Delta Z = Z_{Nd} - Z_Y = 0$, the screened electric potential $\varphi(r)$ is negligible, making the strain difference due to the effective ionic radii (Nd^{3+} and Y^{3+} of 0.1109 nm and 0.1019 nm at 300 K, respectively [23]) dominant. Thus, the Nd concentration $c(x,y)$ will exhibit peaks in the tensile regions of the dislocation cores, followed by pronounced dips in the compressed regions along the GB, and a non-monotonic dependence of $c(x)$ perpendicular to the GB. Equation (1) also shows that the periodic stress $p(y)$ tends to increase the average Nd concentration at the GB, $\langle c\rangle = \int^L c(x,y)dy/L$ where $L \gg d$. For $p_0\Delta V/k_B T \ll 1$, $\varphi = 0$, and $c_0 \ll 1$, and then $\langle c(x,y)\rangle = c_0\langle\exp[-\Delta V p(x,y)/k_B T]\rangle \sim c_0(1 + \Delta V^2\langle p^2\rangle/2{k_B}^2T^2)\rangle\ c_0$, where $\langle p\rangle = 0$, and $\langle p^2\rangle = 2{p_0}^2/[\exp(4\pi\rho/d)-1]$. Taking $\nu = 0.3$, $\mu = 40$ GPa, $\theta = 6°$, we obtain $\Delta V = V_{Nd} - V_Y = 4p({r_{Nd}}^3 - {r_Y}^3)/3$, where r_{Nd} and r_Y are the ionic radii of Nd^{3+} and Y^{3+}, and $T = 300$ K (0.1109 nm and 0.1019 nm, respectively [25]). This leads to the estimated $p_0\Delta V/k_B T \sim 0.85$. The same parameters used in Li *et al* [16] were adapted for the calculations. The predicted segregation profiles for 10% Nd substitution for the 6° and 9° GBs calculated based on the model are depicted in figure 5.

The larger Nd^{3+} is expected to strongly segregate at the GB dislocation cores (compressed regions) with no screened electric potential. Based on the modeling, there is a Nd-depleted zone in the channels between the dislocation cores (figures 5(a) and (b) for 6° and 9° GB, respectively). The expected peak Nd concentration in the equilibrium state reaches as high as 100% (very strong segregation, figures 5(a) and (b)). The strong segregation of Nd^{3+} at the GB dislocation core spontaneously reduces lattice distortion, reducing the strain at the GB and plausibly producing fewer oxygen vacancies than in pure YBCO GB, thus leading to enhanced carrier density and $J_c(H)$ properties as in the case of Ca^{2+} doping [24]. Our results on the transport characteristics of single GBs of $Y_{0.9}Nd_{0.1}Ba_2Cu_3O_{7-d,}$ with segregation of Nd at the core expected from the model provide a clear experimental confirmation of the viability of the isovalent cation doping approach for GB transparency enhancement. Moreover, the expected strong GB segregation of Nd^{3+} implies that smaller doping (less than 10%) can also be highly effective.

For comparison to the experimentally observed segregation for Ca doped films [24], the segregation profiles associated with 10% Ca substitution are depicted for the 6° and 9° GBs in figures 5(c) and (d). For the 6° GB, the degree of segregation for Ca doping is much smaller due to the large contribution of the screened electric potential produced by the substitution of Y^{3+} by anisovalent Ca^{2+}. However, for the 9° GB, there are clear differences in the segregation behavior between Nd and Ca doping (figures 5(b) and (d)). In a previous study of the Ca doping for low-angle GBs [22], it was found that Ca doping in a 9° GB did not significantly enhance $J_{c,gb}$, nor did it eliminate the GB dissipation signature in the *V–I* characteristics, because no segregation (compared to the intra-grain) is anticipated at the 9° GB, as observed from figure 5(d). However, for isovalent Nd^{3+} doping, strong segregation is still expected for 9° GB, which is in agreement with the experimental results of the J_c enhancement (2–5 times) compared to the 9° YBCO GB (figures 5(b) and (d)). Thus, the present study also provides another perspective on the advantages of isovalent Nd doping for the improvement of GB with the angles close to 9°.

Nd doping in YBCO was verified as an effective approach for improving $J_{c,gb}$ without inducing a large T_c reduction. The possible Ba^{2+} site substitution of Nd affected by the growth condition may be the origin of the slight T_c reduction [17], and can be further optimized. Thus, the largest drawback of the GB enhancement by Ca doping, i.e. the strong T_c reduction, was overcome by the newly proposed isovalent cation substitution using Nd ions.

We found that the $Y_{0.9}Nd_{0.1}Ba_2Cu_3O_{7-d}$ compound exhibited different T_c values and different transport characteristics according to the P_{O2} used during the growth of the $Y_{0.9}Nd_{0.1}Ba_2Cu_3O_{7-d}$ films. Even though the highest T_c of ~88 K was obtained at P_{O2} of 300 mTorr, no explicit disappearance of GB dissipation was observed. In this growth condition, Nd segregation may be not favorable, and the Ba^{2+} site substitution may be the smallest as indicated by the least reduction in T_c observed for this sample. However, the other two sample sets grown at 250 mTorr and 200 mTorr exhibited a complete elimination of GB dissipation in their *V–I* characteristics, and a total recovery of $J_{c,gb}$ up to its intra-grain J_c values at a reduced temperature $t \sim 0.85$, even though the T_c values for the samples were slightly lowered to 84 K–86 K. The Nd segregation at cores on scales of a few nm (figures 5(a) and (b)), expected from the segregation model calculation, would relive the strains around the GB cores by expanding the cores, and suppress oxygen vacancies, which is the main cause of the J_c degradation. Nevertheless, these T_c values are much better than the 69 K–80 K of the Ca-doped YBCO [24]. No loss of the GB dissipation signature was found for the 9° GB in these samples; nevertheless, $J_{c,gb}$ improvement by a factor of 2–5 was observed. In these growth conditions, Nd segregation may be more favorable and stable but may be accompanied by larger Ba^{2+} site substitution [23]. Coated conductors based on YBCO became a new enabling technology for efficient electrical power applications nowadays, and this strain-driven segregation may provide another significant strategy to enhance the J_c.

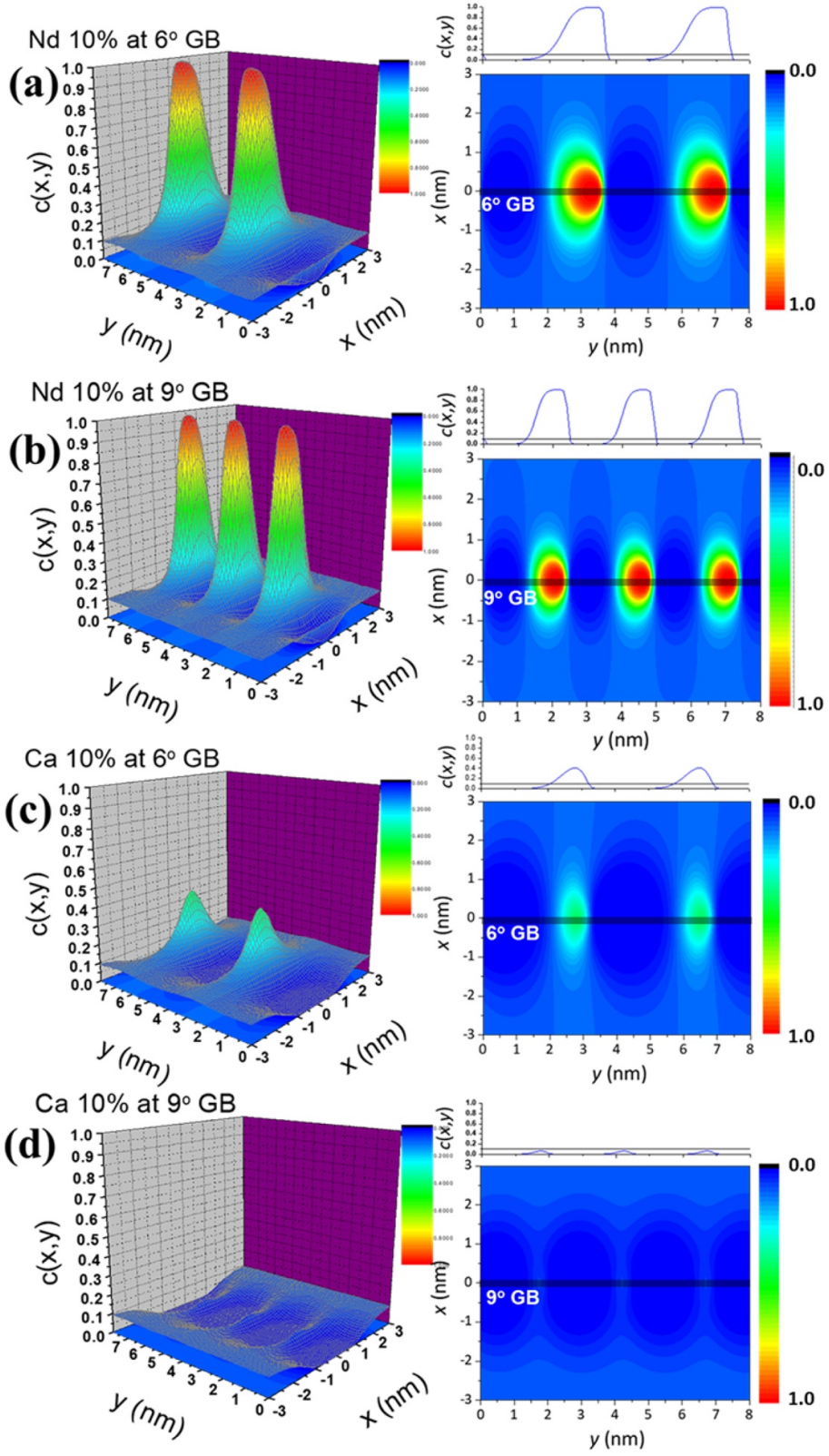

Figure 5. (a) and (b) Surface and contour plots of the concentration of the Nd^{3+} solute ions near a periodic chain of dislocations in a (a) 6° and (b) 9° [001]-tilt GB. $Y_{0.9}Nd_{0.1}Ba_2Cu_3O_{7-d.}$ Very strong segregation is expected in both cases. (c) and (d) surface and contour plots of the concentration of the Ca^{2+} solute ions near a periodic chain of dislocations in a (a) 6° and (b) 9° [001]-tilt GB (for comparison).

5. Conclusion

In this study, we tested the possibility of isovalent Nd doping of YBCO for enhancing GB transparency by measuring the $J_c(H)$ characteristics of quasi-ideal, bicrystal low-angle (6° and 9°) $Y_{0.9}Nd_{0.1}Ba_2Cu_3O_{7-d}$ films. We found that J_c across the 6° GB had the same value as the intra-grain J_c value, while the 9° GB showed a modest J_c enhancement (2–5 times) compared to a pure YBCO 9° GB. As for Ca-doping there was a T_c penalty to be paid but this was significantly smaller with Nd than with Ca. The feasibility of trivalent cation doping in YBCO with a lower T_c reduction than that obtained by the bivalent Ca^{2+} doping was proved. Moreover, the results obtained for the Nd doping in YBCO successfully demonstrated the value of examining the doping of other and perhaps more effective elements such as larger rare-earth ions Gd^{3+}, Eu^{3+}, and Sm^{3+} or some other trivalent ions Y^{3+} substituents.

Acknowledgments

This work was supported by the Air Force Office of Scientific Research at the National High Magnetic Field Laboratory in Tallahassee FL which is also supported by the National Science Foundation under Cooperative Agreements DMR-0654118 and DMR-1644779, by the State of Florida.

ORCID iDs

Sang-il Kim https://orcid.org/0000-0003-0093-720X
David C Larbalestier https://orcid.org/0000-0001-7098-7208

References

[1] Dimos D, Chaudhari P and Mannhart J 1990 *Phys. Rev.* B **41** 4038
[2] Feldmann D M *et al* 2001 *Appl. Phys. Lett.* **79** 3998
[3] Diaz A, Mechin L, Berghuis P and Evetts J E 1998 *Phys. Rev.* B **58** R2960
[4] Heinig N F, Redwing R D, Nordman J E and Larbalestier D C 1999 *Phys. Rev.* B **60** 1409
[5] Gurevich A 2014 *Ann. Rev. Matter Phys.* **5** 35
[6] Kim S I, Feldmann D M, Verebelyi D T, Thieme C, Li X, Polyanskii A A and Larbalestier D C 2005 *Phys. Rev.* B **71** 104501
[7] Feldmann D M, Holesinger T G, Feenstra R and Larbalestier D C 2008 *J. Am. Ceram. Soc.* **91** 1869–82
[8] Chisholm M F and Pennycook S J 1991 *Nature* **351** 47
[9] Babcock S E and Vargas J L 1995 *Annu. Rev. Mater. Sci.* **25** 193
[10] Browning N D, Chisholm M F, Pennycook S J, Norton D P and Lowndes D H 1993 *Physica* C **212** 185
[11] Schmehl A, Goetz B, Schulz R R, Schneider C W, Bielefeldt H, Hilgenkamp H and Mannhart J 1999 *Europhys. Lett.* **47** 110
[12] Hammerl G, Schmehl A, Schulz R R, Goetz B, Bielefeldt H, Schneider C W, Hilgenkamp H and Mannhart J 2000 *Nature* **407** 162
[13] Daniels G A, Gurevich A and Larbalestier D C 2000 *Appl. Phys. Lett.* **77** 3251
[14] Schofield M A, Beleggia M, Zhu Y M, Guth K and Jooss C 2004 *Phys. Rev. Lett.* **92** 195502
[15] Klie R F, Buban J P, Varela M, Franceschetti A, Jooss C, Zhu Y, Browning N D, Pantelides S T and Pennycook S J 2005 *Nature* **435** 475
[16] Li P, Abraimov D, Polyanskii A, Kametani F and Larbalestier D 2015 *Phys. Rev.* B **91** 104504
[17] Salluzzo M, Aruta C, Ausanio G, D'Agostino A and Scotti Di Uccio U 2020 *Phys. Rev.* B **66** 184518
[18] Varanasi C V, Tolliver J C, Haugan T J, Sathiraju S, Maartense I and Barnes P N 2005 *IEEE Trans. Appl. Supercond.* **15** 3722
[19] Song X, Daniels G A, Feldmann D M, Gurevich A and Larbalestier C 2005 *Nat. Mater.* **4** 470
[20] Gurevich A and Pashitskii E A 1998 *Phys. Rev.* B **57** 13878
[21] Mannhart J and Hilgenkamp H 1998 *Mater. Sci. Eng.* B **56** 77
[22] Klie R F, Beleggia M, Zhu Y, Buban J P and Browning N D 2003 *Phys. Rev.* B **68** 214101
[23] Takita K, Akinaga H, Katoh H, Asano H and Masuda K 1988 *Japan. J. Appl. Phys.* **227** L67
[24] Kim S I and Larbalestier D C 2020 *J. Appl. Phys.* **128** 103905
[25] Shannon R D 1976 *Acta Crystallogr.* A **32** 751